Journal of Power Sources 191 (2009) 312–319

Contents lists available at ScienceDirect

Journal of Power Sources

journal homepage: www.elsevier.com/locate/jpowsour

Deterioration of Nafion 115 membrane in direct methanol fuel cells

Se-Jong Shin[a,*], Aliaksandr I. Balabanovich[a], Ho Kim[a], Janghwan Jeong[a], Joohan Song[a], Hee-Tak Kim[b]

[a] Analysis Team, Corporate R&D Center, Samsung SDI Co. Ltd., Gongse-dong, Giheung-gu, Yongin-si, Gyeonggi-do 446-577, Republic of Korea
[b] Energy Development Lab, Corporate R&D Center, Samsung SDI Co. Ltd., Shin-dong, Suwon-si, Gyeonggi-do 443-731, Republic of Korea

ARTICLE INFO

Article history:
Received 22 August 2008
Received in revised form 8 January 2009
Accepted 27 January 2009
Available online 13 February 2009

Keywords:
Membrane
Evolved gas analysis-mass spectrometry
Pyrolysis-gas chromatography–mass spectrometry
Direct methanol fuel cell
Thermal decomposition
Power density

ABSTRACT

A membrane electrode assembly (MEA) based on a Nafion 115 membrane shows a 29% loss in power density after continuous testing in a single direct methanol fuel cell for 1000 h at 50 °C. One of the main reasons for this behaviour is a deterioration of the membrane, namely, its ion-exchange capacity is reduced by 17%. The thermal decomposition behaviour of an untested and degraded membrane is studied by evolved gas analysis-mass spectrometry, pyrolysis-gas chromatography–mass spectrometry, thermo-gravimetric analysis, differential scanning calorimetry, and in situ FTIR reflectance absorption spectra. The results reveal a decrease in thermal stability of the degraded membrane. The Nafion 115 membrane is suggested to lose ion-exchange capacity after the sulfonic acid group is transformed to a thermally less-stable group, such as the persulfonic acid $-SO_2OOH$ group during MEA operation. The structural changes may prevent the formation of ionic clusters.

1. Introduction

Nafion membranes have attracted considerable attention for utilization as a proton conductor in proton-exchange membrane fuel cells (PEMFCs) and direct methanol fuel cells (DMFCs) [1–3]. The development of PEMFCs has been made difficult, however, by the need for a bulky reformer and a heavy storage tank that could be a dangerous system due to a high explosive hazard [4,5]. Operating directly on a liquid methanol fuel, DMFCs are attractive alternative power sources for diverse applications [5–9].

A Nafion membrane is a copolymer consisting of a polytetrafluoroethylene (PTFE) backbone with perfluorinated vinyl ether side-groups that are each terminated with a sulfonic acid group or its salt [1,2]. Since, the membranes are usually operated at 70 °C or higher, their thermal properties and behaviour have been studied extensively [1,3,10–12]. Commonly, for this purpose, thermo-gravimetric analysis (TGA) and differential scanning calorimetry (DSC) have been employed [1].

In the course of long-term operation, DMFCs suffer a power loss. Understanding the reasons for this decline in performance is of considerable importance in the development of more effective DMFCs, therefore serious effort has been mounted in this direction [13]. One possible cause is deterioration of the membrane.

In this work, new methods are suggested to examine the deterioration of a Nafion 115 membrane after 1000 h of testing in a single DMFC. The ion-exchange capacity (IEC) is measured by a potentiometric titration method. In addition to the established thermal analysis techniques of TGA and DSC, evolved gas analysis-mass spectrometry (EGA-MS) and pyrolysis-gas chromatography–mass spectrometry (Py-GC–MS), which determine volatile components during the whole range of decomposition, are applied to characterize untested and degraded membranes. The cause of the decomposition behaviour is discussed.

2. Experimental

2.1. Preparation of membrane electrode assembly (MEA) and operating conditions of DMFC

The MEAs were composed of a cathode gas-diffusion layer (GDL) (SGL 10EA, SGL carbon, Germany), a cathode microporous layer (MPL) (Vulcan XC-72, Cabot, USA), a cathode catalyst layer (Pt-black, HiSPEC 1000, Johnson Matthey, USA), a Nafion 115 membrane (Dupont Corp., USA), an anode catalyst layer (Pt/Ru-black, HiSPEC 6000, Johnson Matthey, USA), an anode MPL (Vulcan XC-72) and an anode GDL (SGL 10AA, SGL carbon, Germany). The MEAs were hot-pressed at about 1200 kPa and a temperature of 125 °C for 3 min [13]. The chemical structure of the Nafion 115 is shown in Fig. 1.

The single cell (Fig. 2) consisted of a bipolar plate and a MEA and was operated with 1 M methanol solution and oxygen at a constant

* Corresponding author. Tel.: +82 41 520 6183; fax: +82 41 560 3073.
E-mail address: ssj622@empal.com (S.-J. Shin).

0378-7753/$ – see front matter © 2009 Elsevier B.V. All rights reserved.
doi:10.1016/j.jpowsour.2009.01.101

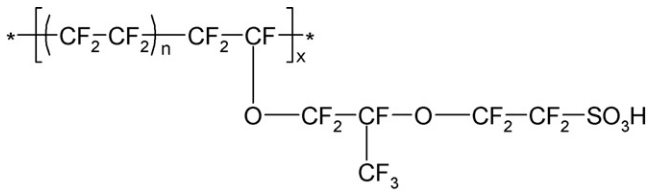

Fig. 1. Chemical structure of Nafion 115.

current of 1.6 A. The operating temperature was between 50 and 70 °C. The anode and cathode reactions were as follows.

$$\text{Anode}: \quad CH_3OH + H_2O \rightarrow CO_2 + 6H^+ + 6e^- \tag{1}$$

$$\text{Cathode}: \quad 3/2O_2 + 6H^+ + 6e^- \rightarrow 3H_2O \tag{2}$$

Even though the thermodynamic cell voltage corresponds to 1.21 V, DMFCs generally show much lower open-circuit voltage due to methanol crossover [14–16].

2.2. Characterization methods

2.2.1. Determination of ion-exchange capacity (IEC)

Clean membranes were removed from the MEAs with a knife and subjected to IEC measurement. The IEC was determined by titrating a dried Nafion membrane stirred in 40 cm^3 of 0.1 M NaCl solution for 24 h to liberate protons. A standardized 0.1 M NaOH solution and a potentiometer (785 DMP Titrino, Metrohm, Switzerland) were employed. Potassium hydrogen phthalate ($KHC_8H_4O_4$, KHP), as a primary standard, was used to acquire the correction factor (F) as given by:

$$F\ (\text{correction factor}) = \frac{\text{KHP (consumed amount, cm}^3) \times 0.1\,\text{M}}{\text{NaOH (consumed amount, cm}^3) \times 0.1\,\text{M}} \tag{3}$$

The IEC is expressed as meq of sulfonic acid groups per gram of dried polymer according to:

$$\text{IEC}\ (\text{meq g}^{-1}) = \frac{\text{NaOH (consumed amount, cm}^3) \times M_{\text{NaOH}} \times F(\text{factor})}{\text{Weight (dried polymer, g)}} \tag{4}$$

2.2.2. EGA-MS

The EGA-MS system consisted of a furnace-type pyrolyzer, PY-2020iD (Frontier Lab., Japan), a GC oven, 6890N (Agilent Technologies, USA), coupled to a mass selective detector (MSD) 5973*inert* (Agilent Technologies, USA) by a short (2.5 m) deactivated EGA capillary tube, UADTM-2.5N (Frontier Lab., Japan) [17]. The furnace (pyrolyzer) was programmatically heated, and the evolved gases produced from a sample were recorded by the MSD on-line after being split at a ratio of 50:1. The MSD provides mass spectral information on the decomposition components of a sample. The technique is similar to thermal gravimetry-mass spectrometry with the signal (total ion chromatogram) corresponding to the first derivative curve of TGA data.

In EGA-MS experiments, a 4 mg sample was placed in a pan and heated from 45 to 600 °C at a heating rate of 10 °C min^{-1} under a helium flow of 1 cm^3 min^{-1}. The temperature of the injector, capillary tube and ion source was held at 280, 300 and 230 °C, respectively. The MSD was applied in an electron impact mode.

2.2.3. Py-GC–MS

The Py-GC–MS system consists of a Curie point pyrolyzer JHP-3 (JAI, Japan) connected to a GC–MS set-up (6890A gas chromatograph-5973*Network* MSD, both Agilent Technologies, USA), in which a HP-5MS capillary column (Agilent Technologies, USA) was used.

The sample was enclosed in a pyrofoil of ferromagnetic metal, which was then placed in the Curie point pyrolyzer [18]. The pyrofoil was rapidly heated to the Curie point temperature of the ferromagnetic metal by radio frequency, and pyrolysis products were released from the sample. The products were carried through the gas chromatographic column to the MSD by a carrier gas.

A 1 mg sample was pyrolyzed at selected temperature for 5 s. The pyrolysis chamber was held at 250 °C and was purged by a helium carrier gas of 50 cm^3 min^{-1} that was split in a ratio of 1:50 before being introduced into the GC. The pyrolysis products were separated on the capillary column using heating rate of 15 °C min^{-1} from 50 to 300 °C. The injector temperature was 280 °C. The MS detector was operated in an electron impact mode at an electron energy of 70 eV with the electron source kept at about 230 °C. The temperature of the GC/MS interface was set at 280 °C.

2.2.4. TGA and DSC

TGA experiments were performed at a heating rate of 10 °C min^{-1} under a nitrogen flow of 50 cm^3 min^{-1} over samples of 10 mg in Pt pans using a TGA 2050 system (TA Instruments, USA).

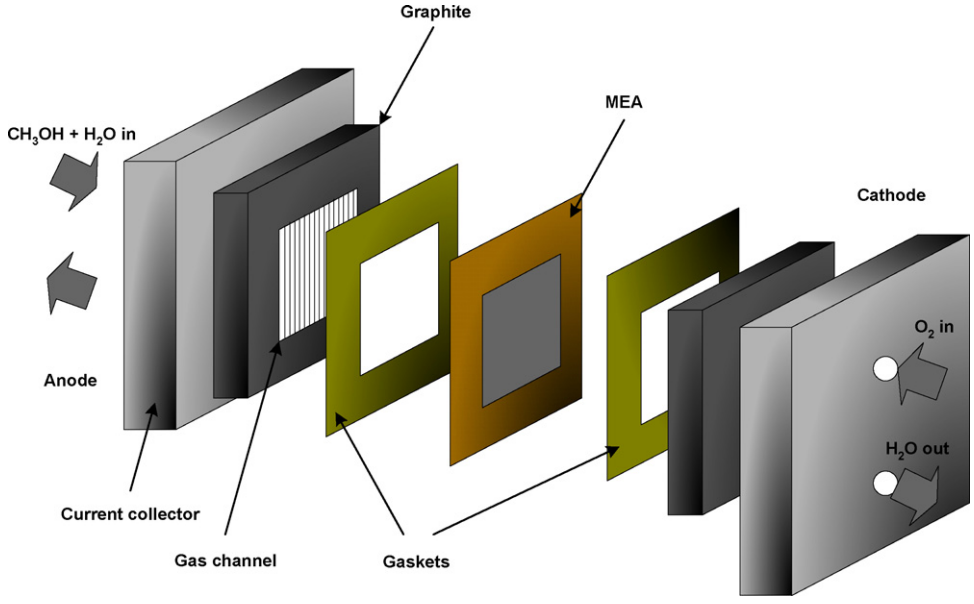

Fig. 2. Illustration of single-cell configuration.

Table 1
IEC of Nafion 115 membranes and power density of MEAs.

Sample	Power density (mW cm^{-2} @ 0.4 V)		IEC (meq g^{-1})
	50 °C	70 °C	
M-I	63	109	0.84
M-1000	45	65	0.70
Nafion 115 (reference)	–	–	0.91

DSC experiments were performed with a 2920 (TA Instrument, USA) set-up. The measurements were conducted at a heating rate of 10 °C min^{-1} under a nitrogen flow of 50 cm^3 min^{-1} using samples of 10 mg placed in aluminum pans.

2.2.5. FTIR

To record changes in IR spectra as a function of temperature, a Nicolet Nexus 870 FTIR spectrometer and a Nicolet Continuum infrared microscope equipped with a Mettler FP82HT hot stage system and a Mettler Toledo FP90 central processor were used. Nafion membranes were placed on a glass slide, covered with a cover slip and heated at 10 °C min^{-1} in the temperature range of 40–360 °C, simultaneously recording IR reflectance absorption spectra with a spectral resolution of 8 cm^{-1} and an average of 32 scans.

3. Results and discussion

3.1. Single-cell performance test and IEC

After continuous operation for 1000 h, the MEA (MEA-1000) was subjected to cell polarization (*I–V* characterization) analysis, and its behaviour was compared with that of an untested MEA (MEA-I). The MEA-I was conditioned for 5 h in a single-cell test apparatus at 80 °C until cell performance was stabilized. The results are presented in Table 1 and Fig. 3. In the comparison with MEA-I, MEA-1000 shows a 29% decrease in power density at 0.4 V and 50 °C.

To corroborate the deterioration of the Nafion 115 membrane, IEC values were measured by means of a potentiometric titration method. As demonstrated in Table 1, three different samples were tested. The IEC value of the Nafion membrane of 1000 h continuous operation (M-1000) is 17% less than that of the untested Nafion membrane (M-I). Nafion 115 (reference), which is the pure membrane, shows the maximum IEC value of 0.91 meq g^{-1}.

To find a possible reason for the deterioration of the membrane, M-I and M-1000 were characterized by the thermal analysis methods of TGA and DSC, together with the new methods of EGA-MS, Py-GC–MS, and FTIR.

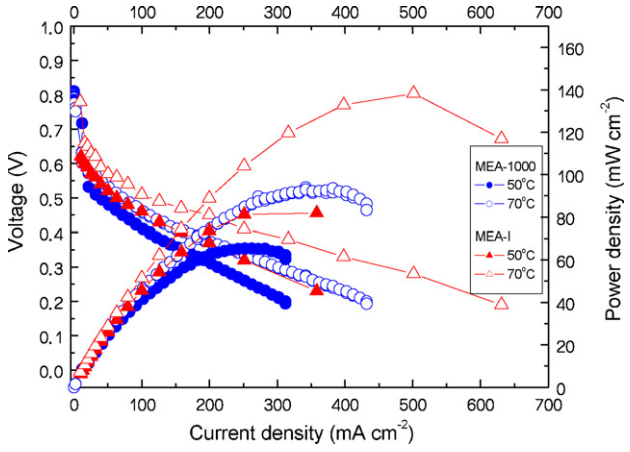

Fig. 3. *I–V* cell performance curves of MEA-1000 and MEA-I at 50 and 70 °C.

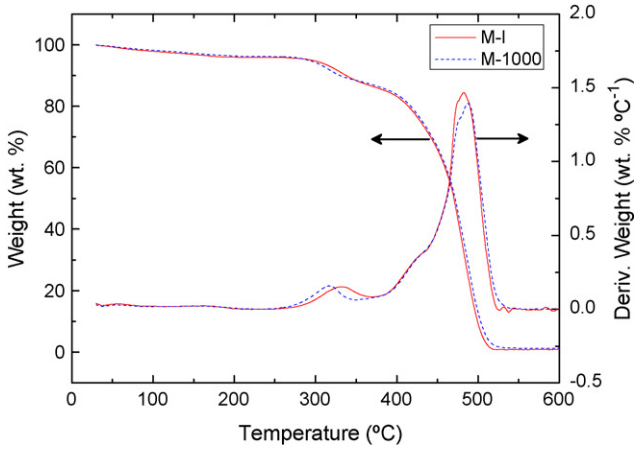

Fig. 4. Thermogravimetry analysis of M-I and M-1000. Runs under a nitrogen flow at a heating rate of 10 °C min^{-1}.

3.2. TGA and DSC

The weight losses of M-I and M-1000 with increasing temperature under a nitrogen flow are presented in Fig. 4. The solid curve is related to the percentage of weight loss, whereas the dashed curve is associated with the first derivative of weight loss. Both of the membranes loose weight in four stages, as revealed from the derivative curves. A four-step weight loss process of Nafion membranes is observed in the TGA curve [19,20].

The first and the second stages are clearly distinguished in the TGA data, whereas the next two stages overlap. According to the literature [21], the first stage of weight loss is related to the release of absorbed water, while the second is associated with the loss of the sulfonic acid groups with a small contribution of side chains. The third stage, which is due to the decomposition of the side chains and the rest of the sulfonic acid groups, overlaps with the backbone decomposition of the fourth stage. The temperature range of each stage and the corresponding amounts of weight loss are presented in Table 2.

M-1000 also exhibits a four-stage weight loss process, but the second stage is shifted in temperature and its derivative maximum is depressed from 270 to 250 °C (Fig. 4). This evidence indicates an earlier decomposition of the sulfonic acid group compared with that of M-I and connects the deterioration from the thermal exposure during the DMFC operation and from the heat generation through the methanol crossover. Also, this shift is confirmed by EGA-MS analysis and is discussed later.

Fig. 5 and Table 3 present the changes in heat flow of M-I and M-1000. The M-I membrane shows two characteristic broad endothermic peaks from 30 to 240 °C. The first peak is associated with the dehydration and the transition of the sample into ionic clusters, followed by crystalline melting of the formed ionomers during the second transition [1]. Furthermore, a sharp complex endothermic phenomenon appears between 240 and 270 °C, which

Table 2
TGA data of Nafion 115 membranes.

Stage	M-I		M-1000	
	Temperature (°C)	Weight loss (wt.%)	Temperature (°C)	Weight loss (wt.%)
1st	30–247	4.0	30–246	3.7
2nd	270–370	8.7	250–350	7.6
3rd and 4th[a]	370–560	14.9	350–542	16.3
	440–560	70.9	440–542	70.1
Residues		1.1		1.5

[a] Overlapped.

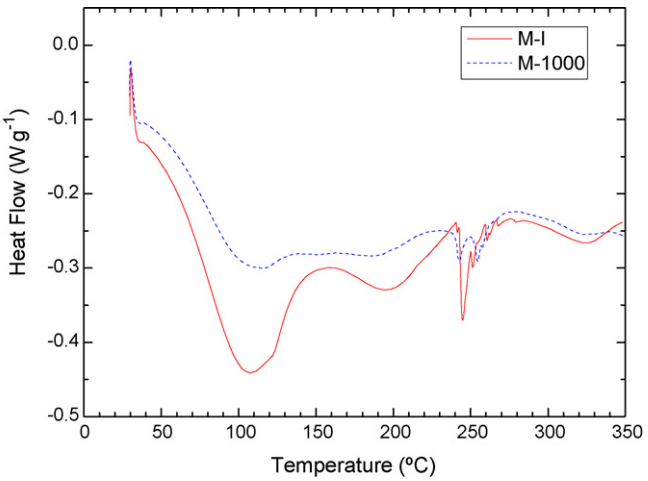

Fig. 5. DSC analysis of M-I and M-1000. Runs under a nitrogen flow at a heating rate of 10 °C min^{-1}.

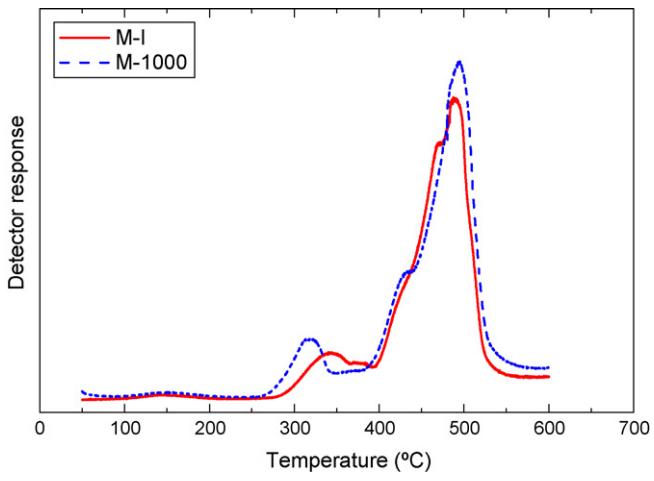

Fig. 6. EGA curves of M-1 and M-1000. Runs under a helium flow at a heating rate of 10 °C min^{-1}.

is reported to be related to the liberation of SO_2 [1]. The next broad endothermic effect in the range of 270–350 °C corresponds to the TGA second stage of weight loss and can be attributed to the loss of SO_2 from the sulfonic acid groups.

The DSC trace of M-1000 reveals that the enthalpies of the first and the second transitions are reduced significantly compared with that of M-I. It is also summarized in Table 3. According to the attributions discussed before, this result suggests that structural changes may occur during operation and prevent the formation of ionic clusters. In addition, the sharp complex peak between 240 and 270 °C is shifted to a lower temperature and becomes better resolved. This behaviour supports the appearance of the structural changes.

3.3. EGA-MS

The total ion EGA curves of M-I and M-1000 are illustrated in Fig. 6. The EGA curves correlate well with the derivative curve of TGA (Fig. 4). There are two main regions of the release of volatile products, namely, 250–370 °C and 370–570 °C. On the other hand, a small stage is also found between 50 and 190 °C. The data in Fig. 6 show that the onset of the first region of M-1000 is lowered, also in accordance with the TGA data.

The selected mass spectra of M-I at three different temperatures are depicted in Fig. 7(a)–(c). Fig. 7(a) portrays the mass spectrum of the evolved products recorded at 342 °C, which corresponds to the maximum value of weight loss during the second stage in TGA. Water and sulfur dioxide are detected by their ions at m/z 18 and 64 (with a fragment ion at m/z 48), respectively. Hexafluoropropene is confirmed by ions at m/z 150, 131, 100, 81, 69, 50 and 31 as the intensity ratio between them is similar to that given in the NIST05 MS library. No oxygen-containing organics are recorded at this stage.

The mass spectra corresponding to the third and fourth stages of weight loss are demonstrated in Fig. 7(b) and (c). In addition to ions due to sulfur dioxide, carbon dioxide and water, a characteristic

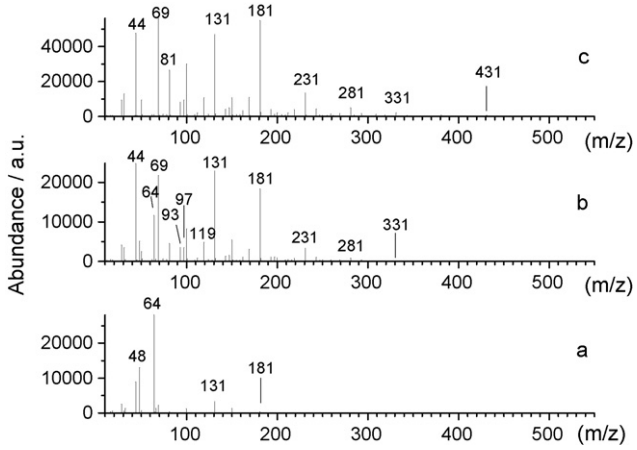

Fig. 7. Mass spectra of evolved products of M-I recorded at (a) 342.3 °C, (b) 422.5 °C and (c) 488.4 °C corresponding to the EGA curve in Fig. 6.

series of perfluorinated organics that can be either true pyrolysis products or originate from MS fragmentation reactions are a feature of these spectra. Those are the series of alkanes, alkenes, dienes, and ketones or unsaturated ethers summarized in Table 4. The latter two series cannot be distinguished by their mass spectra because they have the same molecular formulae.

In an attempt to explain the mass spectra, the NIST05 library was carefully checked. It is found that the mass spectra of perfluorinated vinylalkanes are dominated by the ion at m/z 131 due to $CF_2{=}CF{-}CF_2^+$, whereas the very abundant ion at m/z 181 ($(CF_3)_2C{=}CF^+$) is characteristic of perfluorinated 2-methyl-2-alkenes. In addition to this, perfluorinated alkenes produce fragment ions characteristic of dienes compounds. Furthermore, pefluorinated alkenes give rise to ions at m/z 69, 119, 169 (alkane

Table 3
DSC data of Nafion 115 membranes.

Stage	M-I		M-1000	
	Temperature (°C)	ΔH (J g^{-1})	Temperature (°C)	ΔH (J g^{-1})
1st	104	70.19	99.84	19.74
2nd	199	15.91	193	3.18
3rd	245	4.87	243	0.96
4th	261	0.40	255	1.10
5th	326	5.54	323	1.68

Table 4
Common fragment or molecular ions.

Compound	Ions series	m/z
Alkenes[a]	$CF_2{=}CF{-}(CF_2)_n^+$	81, 131, 181, 231, 281, 331, 381, 431
Alkenes[a]	$C_nF_{4n}^{+\bullet}$ ($M^{+\bullet}$)	100, 150, 200, 250
Alkanes	$CF_3{-}(CF_2)_n^+$	69, 119, 169, 219, 269, 319
Dienes	$C_3F_3(CF_2)_n^+$	93, 143, 193, 243, 293
Dienes	$C_nF_{4n-2}^{+\bullet}$ ($M^{+\bullet}$)	112, 162, 212, 262, 312
C=O-containing	$CF_3{-}(CF_2)_n{-}C{=}O^+$	97, 147, 197, 247, 297
C–O-containing	$CF_2{=}CF{-}(CF_2)_n{-}O^+$	97, 147, 197, 247, 297

[a] Cycloalkanes also give this series.

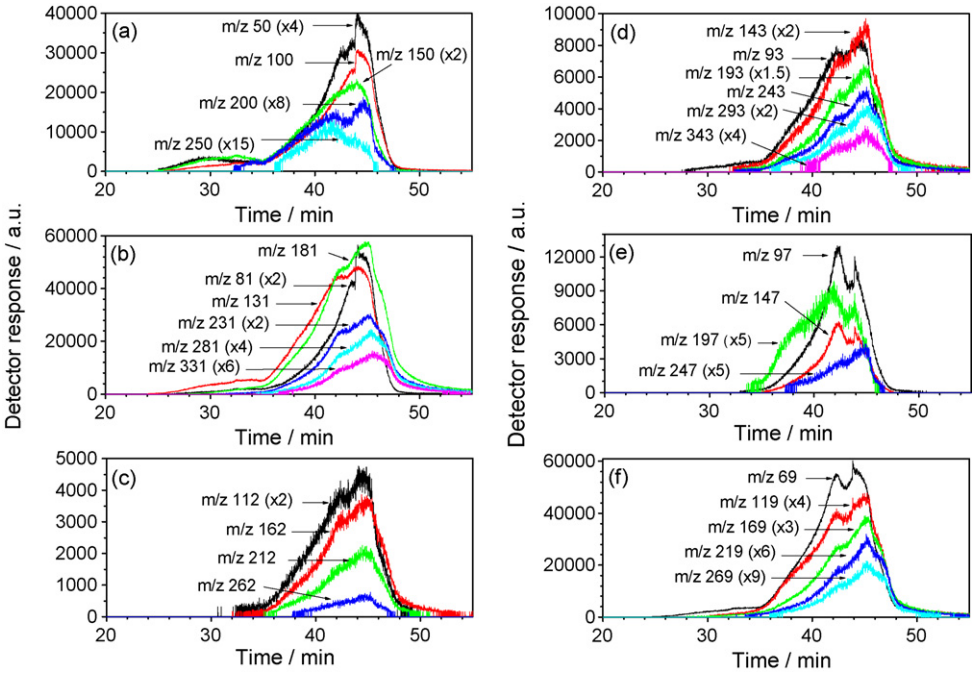

Fig. 8. Extracted profiles for selected ions for: (a) ions at m/z 50, 100, 150, 200, 250 (perflourinated alkene series); (b) ions at m/z 81, 131, 181, 231, 281, 331 (perflourinated alkene series); (c) ions at m/z 112, 162, 212, 262, 312 (perflourinated diene series); (d) ions at m/z 93, 143, 193, 243, 293, 343 (perflourinated diene series); (e) ions at m/z 97, 147, 197, 247, 297 ($C_nOF_{2n-1}^+$ ions series); (f) ions at m/z 69, 119, 169, 219, 269 (perfluorinated alkanes series).

series) but they are less abundant than those of perfluorinated alkanes.

Taking into account the above features of the spectra, it is worth extracting the profiles for selected ions (EPI). Alkenes show two series of ions (Table 4), the EPI of which are illustrated in Fig. 8a and b. Each $C_nF_{2n}^+$ ion of the molecular ion series produces its unique trace in the EPI (Fig. 8a), that differs from those of $C_nF_{2n-1}^+$ ions except for the CF_2CF^+ ion (Fig. 8b). From this evidence, it is concluded that the traces of molecular ions mostly signify the release of perfluorinated alkenes due to pyrolysis, namely, propene, butene and pentene. A trace of tetrafluoroethene (Fig. 8a, m/z = 100) arises from a MS fragmentation of hexafluoropropene at 25–35 min, followed by a CF_2=CF_2 contribution from pyrolysis at 35–48 min to produce a similar profile to the CF_2CF^+ ion (Fig. 8b). Also the $C_nF_{2n-1}^+$ ions exhibit traces that are different from those of the $C_nF_{2n}^{+\bullet}$ ions and this supports an earlier assignment of the cumulative contribution of a variety of ions. For instance, the m/z 131 trace mostly represents the evolution of perfluorinated alkenes and dienes terminating with a –CF=CF_2 group that arise from pyrolysis, whereas the m/z 181 trace mostly denotes the release of alkenes terminating with a –CF=$C(CF_3)_2$ group.

Perfluorinated dienes (Fig. 8c and d) show two series in EPI. The traces of the same number of carbon atoms do not resemble each other closely, thus indicating that they have different sources of origin. The profiles for the molecular ions of C_nF_{2n-2} are likely to signify those of decomposition products, whereas the traces of $C_nF_{2n-3}^+$ ions are due to the cumulative contributions of ions that originate from various product sources.

Oxygen-containing ions (Fig. 8e) generate unique traces signifying that they come from real decomposition products. The $C_2OF_3^+$ (m/z 97) and $C_3OF_5^+$ (m/z 147) ions are characterized by similar evolution profiles that correlate with that of the CF_3^+ ion (Fig. 8f). This is understandable as they originate from the same source, most likely as follows.

$$CF_3–CO–CF_2^+ \rightarrow CF_3–C{=}O^+ \rightarrow CF_3^+ \quad (5)$$

Traces of alkanes are indicated in Fig. 8f. The CF_3^+ ion is manifested by a complex profile that accumulates the ion from various sources: perfluorinated alkenes, alkanes, and oxygen-containing species. Perfluorinated alkenes also contribute to the ions at m/z 119 and 169.

The profile of the pyrolysis products evolves as follows. Water exhibits three stages of release between 0–18, 23–35, and 38–49 min (not shown). The first stage is associated with the release of absorbed water, whereas the next two stages can be related to the decomposition/condensation of oxygen-containing groups (the sulfonic acid group, ether groups). Sulfur dioxide evolves in two stages starting from 23.4 min, with maxima at 29.5 and 37.5 min indicating that there are two types of sulfonic groups in the decomposing Nafion. The evolution of tetrafluoroethene proceeds in one stage between 35 and 50 min. Hexafluoropropene shows two release stages between 25–35 and 35–50 min, that are associated with the decomposition of the side and main chains of Nafion, respectively. In general, perfluorinated alkenes exhibit a complex evolution stage in the range of 35–50 min, where there is also a continuous evolution of perfluorinated dienes and oxygen-containing compounds.

The EGA mass spectra of M-1000 show the same ions as the mass spectra of M-I. In Fig. 9, the selectively extracted ions are compared and are associated with the evolution of (a) sulfur dioxide, (b) oxygen-containing species, (c) mainly perfluorinated propene, and (d) perfluorinated butadiene during pyrolysis of M-I and M-1000. For M-1000, the onset and the maxima of the release of SO_2 are significantly decreased and thereby suggest a decrease in the thermal stability of the membrane. Furthermore, the onset of the release of perfluorinated propene and butadiene, as well as oxygen-containing products, is shifted to a lower temperature, but the effect is less expressed than that of SO_2. In addition, the oxygen-containing moieties released in one step are offset to a higher temperature, which indicates a change in the decomposition mechanism of the M-1000 membrane.

In conclusion, the EGA data reinforce the thermal analysis data in that the M-1000 membrane becomes degraded. Moreover, the

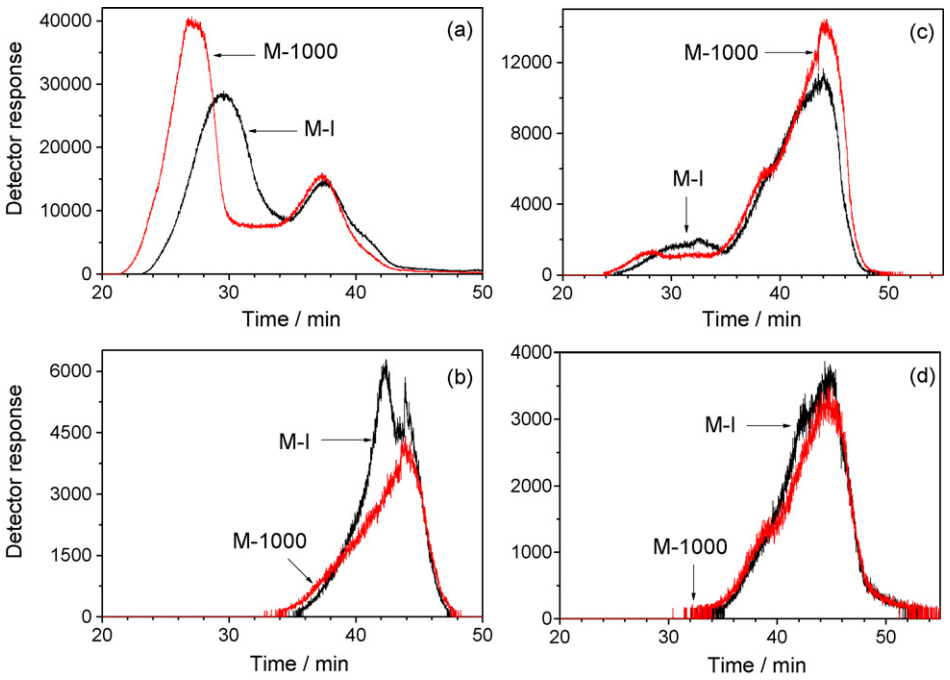

Fig. 9. Selective EGA Extracted profiles for selected ions of M-I and M-1000: (a) *m*/*z* 64 extract ion; (b) *m*/*z* 147 extract ion; (c) *m*/*z* 150 extract ion; (d) *m*/*z* 162 extract ion associated with evolution of sulfur dioxide, oxygen-containing species, mainly perfluorinated propene and perfluorinated butadiene, respectively.

EGA findings reveal that a possible reason for this degradation is associated with deterioration of the sulfonic acid group.

3.4. Py-GC–MS

The M-I sample was initially pyrolyzed at 333 °C. The obtained residue was further subjected to pyrolysis at 445 °C to give a residue which, in its turn, was pyrolyzed at 590 °C.

Fig. 10(a) represents the pyrogram of M-I, related to 333 °C pyrolysis. At this stage, carbon dioxide and sulfur dioxide are proved. The pyrogram obtained at 445 °C (Fig. 10(b)) exhibits a main peak indicative of the formation of sulfur dioxide and hexafluoropropene. In addition, there are minor mass spectral peaks related to low molecular fluorine compounds. A subsequent pyrolysis at 590 °C proves the formation of sulfur dioxide, hexafluoropropene and higher perfluorinated alkenes, as well as perfluorinated oxygen-containing species (Fig. 10(c), base peak). A repeating multiple characteristic of the formation of homologous series follows the base peak. In each multiple, perflourinated alkenes, dienes and oxygen-containing species (several peaks, most likely due to acid fluoride and ketone) are identified.

3.5. FTIR

The in situ FTIR reflectance absorption spectra of M-I recorded at selected temperatures are presented in Fig. 11. Nafion manifests strong absorption bands at 1228 and 1134 cm^{-1} (overlapped) due asymmetric and symmetric CF_2 stretching, and at 983 and 969 cm^{-1} due to C–O–C symmetric stretching [22] (spectrum a). Because of interaction with absorbed water, the sulfonic group gives rise to less intense absorption bands due to SO_3^- ions at 1063 cm^{-1} (symmetric stretching) and 1300 cm^{-1} (asymmetric stretching)

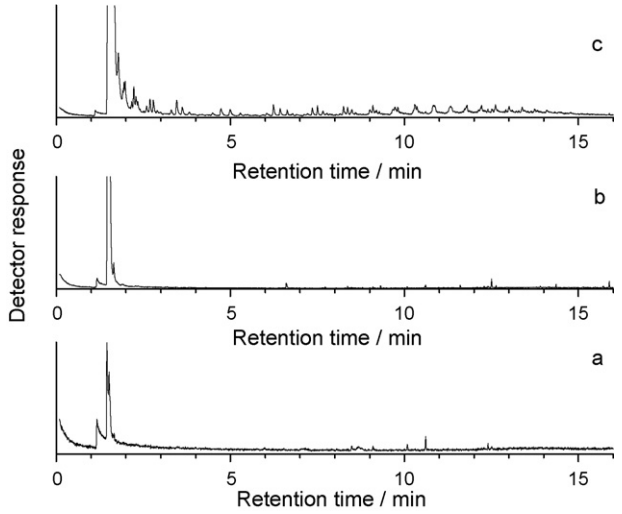

Fig. 10. Pyrograms of M-I obtained by stepwise pyrolysis at (a) 333 °C, (b) 445 °C and (c) 590 °C.

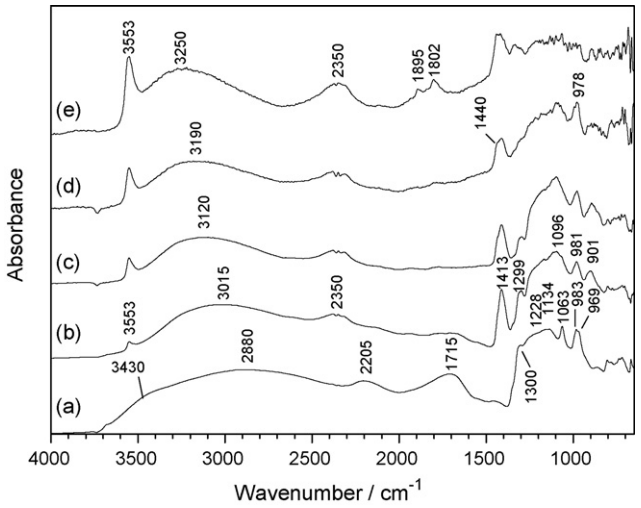

Fig. 11. In situ FTIR reflectance absorption spectra of M-I recorded at (a) 50 °C and (b) 150 °C, (c) 200 °C, (d) 250 °C, (e) 300 °C.

Table 5
Onset (min) of appearance of selected absorption bands in M-I and M-1000.

Sample	Absorption band (cm^{-1})				
	3553	1895	1802	1412	901
Onset time (min)					
M-I	7.3	23.4	22.6	2.0	2.4
M-1000	7.4	22.5	21.7	2.5	2.2

[22,23]. The broad absorption band centred at 2205 cm^{-1} is basically attributed to an overtone of the (OH. . .O) bending mode of oxonium ions enhanced by Fermi resonance [23]. $H_{2n+1}O_n^+$ ions that arise from the interaction of absorbed water and the sulfonic acid group give rise to a broad absorption between 3700 and 1400 cm^{-1} [23].

As discussed in Section 3.2, heating to 150 °C results in the desorption of water that leads to a strong decrease of H_2O and $H_{2n+1}O_n^+$-related absorption bands (spectrum b). In addition, this removal of water affects the position of the absorption bands associated with the SO_3^- ion (the 1063 cm^{-1} band disappears). The 969 cm^{-1} absorption band also decreases. This change in the position of SO_3H and C–O–C-related bands is similar to that noted by studying sorption–desorption processes of water in Nafion [22,23]. Furthermore, the desorption of water results in the appearance of new absorption bands at 1413 cm^{-1} (S=O stretching in the SO_3H group), 901 cm^{-1} (S–O stretching in the SO_3H group) and 3553 cm^{-1} (H–O stretching in the free SO_3H group). The new 2350 cm^{-1} absorption band can be due to an overtone of the (OH. . .H) bending mode of hydrogen-bonded sulfonic acids enhanced by Fermi resonance. The newly formed absorption bands remain on heating up to 300 °C (spectra c–e). The appearance of a shoulder on the 1412 cm^{-1} absorption band is evident in spectrum (d). This new absorption can be associated with the generation of a new S=O-containing compound, probably a sulfonic anhydride. The presence of two sulfonic groups, an acid and an anhydride, can account for the two stages of the release of SO_2, observed in EGA, related to the decomposition of $–SO_3H$ and $–SO_2–O–SO_2–$ groups.

Finally, spectrum (e) denotes the formation of two new absorption bands at 1895 and 1802 cm^{-1} attributed to carbonyl vibration in perfluorinated acid fluorides and ketones, respectively [24,25]. These two absorption bands are indicative of the initiation of degradation processes in the Nafion.

No new absorption bands are found in the FTIR reflectance absorption spectra of M-1000 compared with those of M-I. Nevertheless, a change in the evolution of the bands is noticed. In Table 5, the onset of the rise of selected absorption bands of M-I and M-1000 is shown as a function of time. First and foremost, the onset of the 1895 and 1802 cm^{-1} bands is affected, namely, it decreases from 23.4 and 22.6 min (M-I) to 22.5 and 21.7 min (M-1000). This piece of evidence provides further support for the thermal analysis and EGA data that indicate a decrease in the thermal stability of the M-1000 sample.

3.6. Possible reason for deterioration of M-1000 membrane

Thermal analysis, EGA and FTIR studies reveal that the M-1000 sample is thermally less stable than the M-I counterpart, and this is associated with an earlier decomposition of sulfur-containing groups. One of the reasons responsible for this behaviour may be the partial transformation of the sulfonic acid group during operation of the MEA into a thermally less-stable group, such as the persulfonic acid $–SO_2OOH$ group. This group can appear as a result of the reaction of hydrogen peroxide (which is generated during the course of operation of MEA) with the $–SO_2OH$ group [26]. Consequently, the decomposition products of the persulfonic acid group can initiate degradation of the ether bonds of Nafion. It is possible that development of the $–SO_2OOH$ groups results in a decrease in power density.

Alternatively, it can be speculated that reduction of the sulfonic acid group on the surface close to anode can occur by hydrogen catalyzed by Pt. As pointed out by Firouzabadi and Jamalian [27], the reduction of the sulfonic acid group in contrast to other sulfonyl groups is a very difficult process.

4. Conclusions

In a single-cell performance test of a DMFC at 0.4 V and 50 °C, a 1000-h operated MEA shows a 29% loss in power density compared with an untested MEA. Deterioration of the Nafion 115 membrane is one of the main reasons for the decrease in power density; it shows a 17% loss in the IEC value. Thermal analysis, EGA and FTIR data reveal that the deteriorated membrane suffers from a loss in thermal stability caused by an earlier decomposition of the sulfur-containing groups. The accumulation of persulfonic acid groups during operation of the MEA may be responsible for this behaviour.

References

[1] S.H. de Almeida, Y. Kawano, Thermal behavior of Nafion membranes, J. Therm. Anal. Calorim. 58 (1999) 569–577.
[2] Z. Liang, W. Chen, J. Liu, S. Wang, Z. Zhou, W. Li, G. Sun, Q. Xin, FT-IR study of the microstructure of Nafion® membrane, J. Membr. Sci. 233 (2004) 39–44.
[3] A.-L. Rollet, O. Diat, G. Gebel, A new insight into Nafion structure, J. Phys. Chem. B 106 (2002) 3033–3036.
[4] S. Hikita, K. Yamane, Y. Nakajima, Measurement of methanol crossover in direct methanol fuel cell, Soc. Autom. Eng. Jpn. 22 (2001) 151–156.
[5] Y. Woo, S.Y. Oh, Y.S. Kang, B. Jung, Synthesis and characterization of sulfonated polyimide membranes for direct methanol fuel cell, J. Membr. Sci. 220 (2003) 31–45.
[6] S.-J. Shin, S.-R. Choi, H.-J. Kim, B.-R. Min, Synthesis and characterization of poly (arylene ether) sulfone for direct methanol fuel cell, ICOM 2005 PM-096, in: International Congress on Membranes and Membrane Processes, Seoul, Korea, 2005, p. II-1013.
[7] G.S. Kang, H.-H. Namkung, Y.-R. Kim, S.-J. Im, S.-J. Shin, H.-J. Kim, J.-P. Kim, B.-R. Min, Preparation and characterization of chitosan membranes: effect of addition agent on the membrane properties, ICOM 2005 PM-083, in: International Congress on Membranes and Membrane Processes, Seoul, Korea, 2005, p. II-987.
[8] S.-J. Shin, J.-P. Kim, H.-J. Kim, J.-H. Jeon, B.-R. Min, Preparation and characterization of polyethersulfone microfiltration membranes by a 2-methoxyethanol additive, Desalination 186 (2005) 1–10.
[9] S.J. Im, R. Partel, S.J. Shin, J.H. Kim, B.R. Min, Sulfonated poly(arylene ether sulfone) membranes based on biphenol for direct methanol fuel cells, Korean J. Chem. Eng. 25 (2008) 732–737.
[10] W. Vielstich, A. Lamm, H.A. Gasteiger, Handbook of fuel cells, vol. 3, Wiley, Chichester, 2003, pp. 647–662.
[11] J. Chou, E.W. McFarland, H. Metiu, Electrolithographic investigations of the hydrophilic channels in Nafion membranes, J. Phys. Chem. B 109 (2005) 3252–3256.
[12] S. Banerjee, D.E. Curtin, Nafion® perfluorinated membranes in fuel cells, J. Fluorine Chem. 125 (2004) 1211–1216.
[13] H. Kim, S.-J. Shin, Y.-G. Park, J. Song, H.-T. Kim, Determination of DMFC deterioration during long-term operation, J. Power Sources 160 (2006) 440–445.
[14] V.S. Silva, A. Mendes, L.M. Madeira, S.P. Nunes, Proton exchange membranes for direct methanol fuel cells: properties critical study concerning methanol crossover and proton conductivity, J. Membr. Sci. 276 (2006) 126–134.
[15] A. Heinzel, V.M. Barragan, A review of the state-of-the-art of the methanol crossover in direct methanol fuel cells, J. Power Sources 84 (1999) 70–74.
[16] Y.-J. Kim, B. Bae, M.A. Scibioh, E. Cho, H.Y. Ha, Behavioral pattern of a monopolar passive direct methanol fuel cell stack, J. Power Sources 157 (2006) 253–259.
[17] K. Kadokami, K. Tanada, K. Taneda, K. Nakagawa, Novel gas chromatography–mass spectrometry database for automatic identification and quantification of micropollutants, J. Chromatogr. A 1089 (2005) 219–226.
[18] S. Nakamura, M. Taguchi, S. Naniwada, N. Ohguri, Specimen capsule and process for gas chromatography, US Patent 3,992,174 (1976).
[19] I.D. Stefanithis, K.A. Mauritz, Microstructural evolution of a silicon oxide phase in a perfluorosulfonic acid ionomer by an in situ sol–gel reaction. 3. Thermal analysis studies, Macromolecules 23 (1990) 2397–2402.
[20] C.A. Wilkie, J.R. Thomsen, M.L. Mittleman, Interaction of poly(methyl methacrylate) and Nafions, J. Appl. Polym. Sci. 42 (1991) 901–909.
[21] L. Sun, J.S. Thrasher, Studies of the thermal behavior of Nafion® membranes treated with aluminum (III), Polym. Degrad. Stabil. 89 (2005) 43–49.
[22] M. Falk, Perflourinated ionomer membranes, in: A. Eisenberg, H.L. Yeager (Eds.), ACS Symposium Series 180, ACS, Washington, DC, 1982, pp. 139–170.

[23] R. Buzzoni, S. Bordiga, G. Ricchiardi, G. Spoto, A. Zecchina, Interaction of H_2O, CH_3OH, CH_3CN, and pyridine with the superacid perfluorosulfonic membrane Nafion: An IR and Raman study, J. Phys. Chem. 99 (1995) 11937–11951.
[24] K.R. Loos, R.C. Lord, Vibrational spectrum and barrier to internal rotation for CF_3CFO, Spectrochim. Acta 21 (1965) 119–125.
[25] C.J. Pouchert, The Aldrich Library of FT-IR Spectra, Vapor Phase, vol. 3, first ed., Aldrich Chemical Company, Bruxelles, 1989.
[26] W.F. Hoelderin, F. Kollner, in: J.J. Spivey (Ed.), Catalysis, Royal Society of Chemistry, Cambridge, 2002, pp. 43–66.
[27] H. Firouzabadi, A. Jamalian, Reduction of oxygenated organosulfur compounds, J. Sulfur Chem. 29 (2008) 53–97.